A Lookup Table Based Loss Minimizing Control for FCEV Permanent Magnet Synchronous Motors

Jung-Gi Lee*, Kwang-Hee Nam*, Sun-Ho Lee*, Soe-Ho Choi and Soon-Woo Kwon****

Abstract – A loss minimizing controller is developed for a fuel cell electric vehicle (FCEV) permanent magnet synchronous motor (PMSM). The PMSM losses are modeled by some experimental equations. Applying Lagrangian to the loss function, a necessary condition for the optimality appears to be a fourth order polynomial, and the loss minimizing solutions are obtained by a simple numerical approach. On the other hand, the loss minimizing solutions are found by scanning the motor loss in the entire operating region. The two results agree well. The loss minimizing current sets for given torque and speed are made into a table, which is utilized as a look-up in the current control loop.

Keywords: PMSM, Loss minimization, FCEV

1. Introduction

Due to high efficiency and high power of weight ratio PMSMs are preferred for power propulsion in electric vehicles. High efficiency is particularly important in hybrid electric vehicle (HEV) and FCEV, since it is directly related to the battery size, vehicle size/weight, and vehicle cost.

PMSMs are more efficient than induction motors, since nocurrent is necessary for rotor flux generation. Hence, copper loss is relatively low in PMSMs[1]. Normally, automotive PMSMs have low slot numbers per pole per phase. Further, contrary to industry application, there are strong limits in the motor volume and weight, and as a result, the stator flux density is designed to be relatively high. Therefore, in the high current operation, the stator core is partly saturated and even cross coupling takes place between d and q-axis current.

The motor losses consist of mechanical loss, copper loss, iron loss, and stray loss. As the torque and speed increase, current and voltage are utilized maximally. Hence, the loss minimizing solution is obtained either in the interior or on the current/voltage limits.

Nakamura et al.[2] utilized the fact that high efficiency was obtained at the unity power factor condition in the design of a controller for the PMSM. Morimoto et al.[3] established a loss minimizing control based on an equivalent circuit which contained an iron loss model, as well as a copper loss model. Taking differentiation of the loss function, the d-axis current yielding the minimum loss is obtained.

Mademlis and Margaris[4] formulated a loss function in a quadratic form of d and q-axis current, and derived an analytic loss minimizing solution. Fernandez-Bernal et al.[6] proposed a method of estimating the resistances that reflect the iron and copper losses. Cavallaro et al[7]. developed an on-line loss minimizing algorithm based on the work of Morimoto et al.[3]. According to their algorithm, d-axis current is adjusted until the electrical input power settles down to the lowest value for a given torque and speed.

Gallegos-Lopez et al.[8] considered an optimum torque control of PMSM in the field weakening region with a focus on automotive application. In the low speed region, maximum torque per ampere (MTPA) was utilized in the low speed region, and in the field weakening region, the maximum power solution was found on the current limit circle, or on the voltage limit curves. However, loss minimization that included the iron loss was not specifically dealt. Jeong et al.[9] considered field saturation and cross coupling in the copper loss model, and applied Newton's method in search of the minimum loss current commands in the control loop. But, these kinds of online numerical methods seem to cause computational burden and complexity in implementation. Further, investigation of optimality on the boundary lacks.

Bianchi et al.[12] utilized an experimental search method in obtaining an MTPA solution. An interior permanent magnet motor design considering both motor and inverter cost was studied by Lovelace et al.[13]. Haddoun et al.[14] derived a loss model for an electric vehicle (EV) induction motor, and chose the ratio between d and q axes current as a control variable in the optimal value search. The resulting optimum condition was that the loss of d and q axes must be the same. Shinnaka and Sagawa [15] studied an optimal control method for PMSM which has an extra winding on the rotor.

The aim of this work is to develop a look-up table based loss minimizing control law for a FCEV motor. The DC link voltage of FCEV is subject to change, since the fuel cell (FC) output voltage varies depending on load current, stack temperature, humidity, air pressure, etc. An optimal look-up table with a recursive algorithm which accommodates varying DC link voltage is proposed.

* Dept. of Electrical and Electronic Engineering, Pohang University of Science and Technology POSTECH University, Pohang 790-784 Korea.(baabu@postech.ac.kr; kwnam@postech.ac.kr; lsh1207@postech.ac.kr)

** HYUNDAI Motor Company, Yongin 446-912, Korea. (seoho@hyundai-motor.com ; kingksw@hmc.co.kr)

Received 4 June 2008; Accepted 23 January 2009

2. PMSM Dynamic and Loss Models

2.1 FCEV Motor Requirements and Loss Model

The use of electric motor as the main driving power source has several advantages: Full torque operation is possible from the standstill. In addition, since the motor speed range is wide, clutch and gear shift are not needed. Short time overload is 2 times higher than the nominal torque. Due to this overload capacity, the response is much faster than internal combustion engine.

Since the motor power is equal to the product of torque and speed, either torque or speed has to be increased to make the motor power high. But since the rated torque is proportional to the rotor volume, EV motors tend to have high base speed in order to reduce the motor volume and weight. Nowadays, the maximum FCEV motor speed is increased as high as 12,000rpm. Note that 12,000rpm is nearly the peak speed that roll bearings can endure in the 100kW power range. On the other hand, the EV motors should have a high starting torque. Specifically, the rated torque should be high enough to start the vehicle on 30 % grade slope. Therefore, EV motors normally have 6 or 8 pole structure. These two facts imply that EV motors have a very wide constant power speed range (CPSR), i.e., they should be designed to have a wide field weakening range.

2.2 PMSM Dynamic Model

Voltage equations for a PMSM in the synchronous frame are given by

$$v_d = r_s i_d + \frac{d\lambda_d}{dt} - \omega\lambda_q \quad (1)$$

$$v_q = r_s i_q + \frac{d\lambda_q}{dt} + \omega\lambda_d \quad (2)$$

where i_d ,(i_q), v_d,(v_q) and ω are d(q)-axis current, d(q)-axis voltage, d(q)-axis flux linkage, and electrical angular velocity. Flux is assumed to be linear in current such that $\lambda_d = L_d i_d + \psi_m$, and , $\lambda_q = L_q i_q$, where $L_d(L_q)$ is d(q) axis inductance and ψ_m is the rotor flux from permanent magnets. Neglecting ohmic voltage drops and assuming the steady state, we have

$$v_d = -\omega L_q i_q \quad (3)$$

$$v_q = \omega L_d i_d + \omega\psi_m \quad (4)$$

The electromagnetic torque is given by:

$$T_e = \frac{3p}{4}(\psi_m i_q + (L_d - L_q) i_d i_q) \quad (5)$$

where p is the pole number.

2.3 PMSM Loss Model

The PMSM loss consists of copper loss, iron loss, stray loss, and mechanical loss such as windage loss. Since the windage loss is not directly related to the motor current or flux level, it is not dealt here.

- Copper Loss: Copper loss is caused by the stator coil resistance r_s:

$$P_{cu} = \frac{3}{2} r_s I^2_s = \frac{3}{2} r_s (i^2_d + i^2_q) \quad (6)$$

- Iron Loss: Iron loss consists of hysteresis loss and eddy current loss. The former is estimated according to $k_h B^\beta \omega$, where β is the Steinmetz constant. The later depends on the square of the frequency, i.e., $k_e B^2 \omega^2$. Typical values for grades of silicon iron laminations used in small and medium motor, with the stator frequency given in radians per second, are in the ranges k_h = 40~55, k_e = 0.04~0.07 and β = 1.8~2.2 [1]. However due to the differences in flux density and volume, the iron losses in the teeth and core are calculated separately. An empirical formula for iron loss is given by

$$P_{fe} = c_{fe} \omega^\gamma (\lambda^2_d + \lambda^2_q) \quad (7)$$

where γ =1.5 ~1.6 and c_{fe} =1.5~1.6 [10]

- Stray Loss: The stray losses are due to the higher winding space harmonics and slot harmonics. These losses are in the surface layers of the stator and rotor adjacent to the air gap and in the volume of the teeth. The calculation of stray losses is difficult and does not guarantee a satisfactory accuracy. In practice, the stray losses are evaluated as [5]

$$P_{str} = c_{str} \omega^2 (i^2_d + i^2_q) \quad (8)$$

where c_{str} is the stray loss coefficient.

Summing the above losses, the total loss P_t is equal to

$$P_t = P_{cu} + P_{fe} + P_{str} \quad (9)$$
$$= k_1 i^2_d + k_2 i^2_q + k_3 i_d + k_4$$

where $k_1 = \frac{3}{2} r_s + c_{fe} \omega^\gamma L^2_d + c_{str} \omega^2$

$k_2 = \frac{3}{2} r_s + c_{fe} \omega^\gamma L^2_q + c_{str} \omega^2$

$k_3 = 2 c_{fe} \omega^\gamma L_d \psi_m$

$k_4 = c_{fe} \omega^\gamma \psi^2_m$

3. Loss Minimizing Solution

The MTPA gives the current vector of minimum magnitude among the solutions which yield a specified torque. Thus, it can be interpreted as the copper loss minimizing solution. Note that MTPA is independent of the frequency ω. Therefore, MTPA is not related to the iron loss and the stray loss that have strong dependence on ω_r.

Note from (5) that torque T_e is a function of i_d and i_q. To produce a certain level of torque, there are numerous choices for (i_d, i_q). But, motor loss P_t is not the

same in various cases. The problem here is to find a set of current components that minimizes the loss. The loss minimizing control (LMC) is targeted to obtain a desired current set (i_d, i_q) that minimizes P_t for a given torque value T_0 and speed ω_r.

The voltage constraint is obtained from (3) and (4) such that

$$v_d^2 + v_q^2 = (L_d i_d + \psi_m)^2 \omega^2 + \omega^2 (L_q i_q)^2 \le V_{\max}^2 \quad (10)$$

Note that $V_{\max} = V_{DC}/\sqrt{3}$, where V_{DC} is the inverter DC link voltage. The magnitude of rotor flux linkage is equivalently expressed as a product of L_d and a virtual current source i_f, i.e. $\psi_m = L_d i_f$. The voltage limit (10) appears as an ellipse in the (i_d, i_q) plane:

$$\frac{(i_d + i_f)^2}{V_{\max}/\omega^2 L_d^2} + \frac{i_q^{\,2}}{V_{\max}/\omega^2 L_q^2} \le 1 \quad (11)$$

With the current limit and voltage limit, the loss minimization is formulated as

Minimize $P_t(i_d, i_q)$

$$\text{Subject to } \frac{3P}{4}(\psi_m i_q + (L_d - L_q) i_d i_q) - T_0 = 0 \quad (12)$$

$$(L_d i_d + \psi_m)^2 \omega^2 + \omega^2 (L_q i_q)^2 \le V_{\max}^2 \quad (13)$$

$$i_d^2 + i_q^2 \le I_{\max}^2 \quad (14)$$

Since the LMC problem is an optimization under inequality constraints, one needs to apply Kuhn-Tucker theorem [17]. However, the cases of optimal point occurring at a boundary are straightforward from the view of physical insight. Thus, we only consider solving the optimization problem in interior points. Let the Lagrangian be defined by

$$L(i_d, i_q) = P_t(i_d, i_q) + \mu(T_e - T_0)$$

where μ is a Lagrangian multiplier. Necessary conditions for the existence of the optimal solution are

$$\frac{\partial L(i_d, i_q)}{\partial i_d} = 3 r_s i_d + 2 c_{str} \omega^2 i_d + 2 c_{fe} \omega^\gamma L_d^2 i_d + 2 c_{fe} \omega^\gamma L_d \psi_m + \mu \frac{3P}{4}(L_d - L_q) i_q = 0 \quad (15)$$

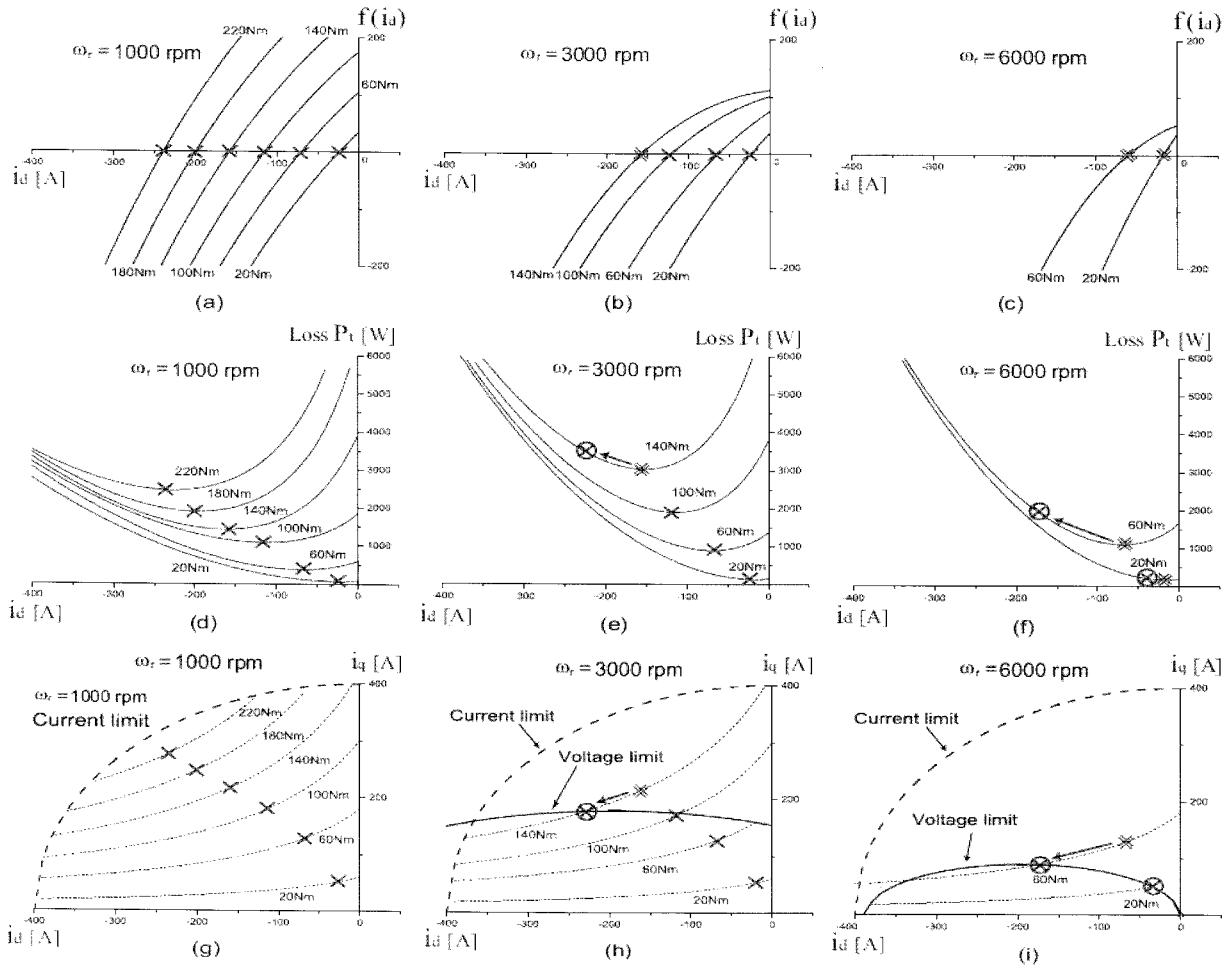

Fig. 1. Calculated results illustrating how to find the loss minimizing (i_d, i_q) for three different speeds: (a), (b), and (c): plot of $f(i_d)$ for different torques, (d), (e), and (f): power loss curves along constant torque contours (g), (h), and (i): constant torque contours in the (i_d, i_q) plane.

$$\frac{\partial L(i_d,i_q)}{\partial i_q} = 3r_s i_q + 2c_{str}\omega^2 i_q + 2c_{fe}\omega^{\gamma} L_q^2 i_q + \mu\frac{3P}{4}\psi_m + \mu\frac{3P}{4}(L_d - L_q)i_d = 0 \quad (16)$$

Eliminating μ from (15) and (16) and replacing i_q by utilizing (12), we obtain again a fourth order equation:

$$f(i_d) \equiv Ai_d^4 + Bi_d^3 + Ci_d^2 + Di_d + E = 0 \quad (17)$$

where

$$A = \frac{27P^3}{64}(L_d - L_q)^3(3r_s + 2c_{str}\omega^2 + 2c_{fe}\omega^{\gamma}L_d^2)$$

$$B = \frac{27P^3}{64}\psi_m(L_d - L_q)^2(9r_s + 6c_{str}\omega^2 + 6c_{fe}\omega^{\gamma}L_d^2) + 2(L_d - L_q)c_{fe}\omega^{\gamma}L_d^2)$$

$$C = \frac{27P^3}{64}\psi_m^2(L_d - L_q)(9r_s + 6c_{str}\omega^2 + 6c_{fe}\omega^{\gamma}L_d^2) + 6(L_d - L_q)c_{fe}\omega^{\gamma}L_d^2)$$

$$D = \frac{27P^3}{64}\psi_m^3(3r_s + 2c_{str}\omega^2 + 2c_{fe}\omega^{\gamma}L_d^2) + 6(L_d - L_q)c_{fe}\omega^{\gamma}L_d^2)$$

$$E = \frac{27P^3}{64}\psi_m^4 c_{fe}\omega^{\gamma}L_d - \frac{9P}{4}(L_d - L_q)r_s T_0^2 - \frac{3P}{2}(L_d - L_q)c_{str}\omega^2 T_0^2) - \frac{3P}{2}(L_d - L_q)c_{str}\omega^{\gamma}L_q^2 T_0^2)$$

Note that all coefficients contain ω, and that E includes torque T_0. Hence, the solution for $f(i_d) = 0$ is different for each (T_0, ω). Pan and Sue [11] also obtained another fourth order equation in id. However, in general, it is very difficult to obtain a solution for a fourth order polynomial in a closed form. In this work, we utilize a numerical method.

Fig. 1 (a), (b), and (c) show the plots of (17) for different torque and speed. They appear as straight functions in the region where $i_d < 0$, so that it is easy to find the zero crossing points which were marked by '×'. The second row of Fig. 1 shows the curves of motor losses P_t versus i_d along the constant torque lines. The loss curves were calculated by utilizing (9) and (5). It should be noted that P_t has the minimum values at the values of i_d where function f crosses zero, as predicted by the necessary conditions (12), (15), and (16) for optimality. The third row of Fig. 1 shows the plots of constant torque curves in the current plane with current and voltage limits. The optimal points are also marked by '×'. However, as the speed increases, the voltage limit curve shrinks. As a result, some solutions where located out of the voltage limit, and marked by double '×'. Those points should be replaced by the points on the boundary. That is, in such cases the solution is found on an intersection of the voltage limit ellipse and the torque parabola [8], [11]. The solution on the boundary was marked by '⊗'. Table 1 shows an EV motor data used in this calculation and the following experiments.

Table 1. Parameters of a PMSM for FCEV

Input DC link voltage[V]	240
Maximum Speed [rpm]	11000
Maximum/rated output power[kW]	80/40
Maximum/rated phase current [A]	400/216
d axis inductance (L_d) [μH]	375
q axis inductance (L_q) [μH]	835
Stator resistance (r_s) [$m\Omega$]	9.5
Permanent magnet flux (ψ_m) [Wb]	0.074
Number of pole (p)	6
Number of stator slot	54
Switching frequency [kHz]	8

3.1 Construction of LMC Look-up Table

A collection of loss minimizing (i_d, i_q) needs to be prepared for the table look-up in the torque control loop for the PMSM of a FCEV. In the following, an algorithm of generating the loss minimizing (i_d, i_q) sets, i.e., LMC look-up table is summarized:

For a given speed ω^j, choose a feasible torque T_e^k from the torque speed curve, where 'feasible' means that a solution exists within the voltage and current limits. For ω^j, we denote the region inside a voltage limit by

$$U_V^j = \{(i_d, i_q) \mid (L_d i_d + \psi_m)^2 + (L_q i_q)^2 \le \frac{V_{\max}^2}{\omega_j^2}\}$$

where $V_{\max} = V_{DC}/\sqrt{3}$. A procedure for generating the LMC table consists of two parts: finding the loss minimizing solutions from interior points, and obtaining solutions on the boundary.

(A1)

i) Calculate the coefficients $A \sim E$ of function f utilizing (ω_i, T_e^j);

ii) Plot $f(i_d)$ and find a zero crossing value, i_d^{jk}.

iii) Obtain q-axis current corresponding to i_d^{jk}:

iv) Check whether or not the current pair satisfies the voltage limit condition, i.e., check $(i_d^{jk}, i_q^{jk}) \in U_V^j$.

If the solution is outside of the voltage limit, then the solution should be extrapolated to the boundary along the constant torque curve and the optimal solution is found on an intersection point between the torque and the voltage limit curves. When there are two intersection points, the left side solution will be the optimal since it has a shorter length.

A method of finding the boundary optimal solution from (i_d^{jk}, i_q^{jk}) can be summarized as:

(A2)

i) Let $i_d^{jk'} = i_d^{jk} - \Delta i_d$;

ii) Find the corresponding q-axis current utilizing

$$i_d^{jk'} = \frac{4/(3P)T_e}{\psi_m + (L_d - L_q) i_d^{jk'}}$$

iii) Check whether $(i_d^{jk}, i_q^{jk}) \in U_V^j$. If 'yes', stop. If 'no', let $(i_d^{jk}, i_q^{jk}) = (i_d^{jk'}, i_q^{jk'})$, and go to Step i).

As we run (A2), the point moves to the left along the constant torque line T_e^j to the point where the torque line intersects the voltage limit curve.

Repeating algorithms (A1) and (A2) for all feasible (T_e^k, ω_r) under the speed and current limits, we can construct a look-up table of the optimal current pairs.

3.2 LMC Table for Reduced DC Link Voltage

FC output voltage changes depending on the load current, FC temperature, air pressure, humidity level, etc[16]. The voltage dependence on the current density is described by the polarization curves of FCs.

The LMC look-up table should be properly adjusted for different DC link voltages. As the DC link voltage is reduced, some interior optimal points calculated for a high DC link voltage will be excluded outside of the voltage limit. In such a case, the optimal point should be relocated at the boundary.

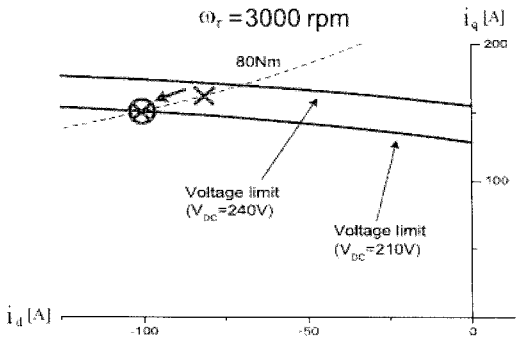

Fig. 2. Optimal point migration from A to B as the DC link voltage reduces.

Fig. 2 shows that point A which was inside the voltage limit when V_{DC} = 240V is excluded by a reduced voltage ellipse (V_{DC} = 210V). In this case, the point needs to be replaced by point B on the boundary. Note that both points A and B are on the same torque line (80 Nm). For a reduced DC link voltage, one may utilize algorithm (A2) as a method of finding the intersection point. Note that the intersection point is another optimal point under the reduced DC link voltage.

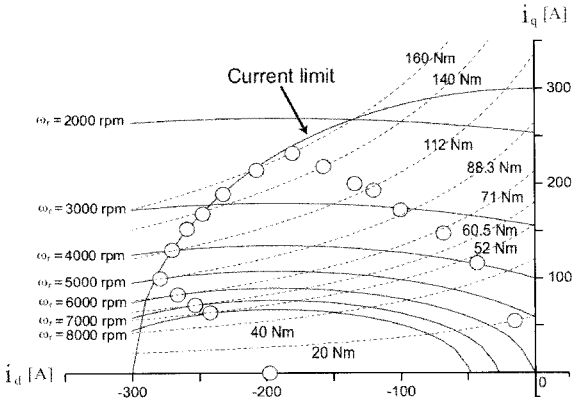

Fig. 3. Loci of maximum torque and maximum power operations in the current plane.

Fig. 3 shows the loci of maximum torque and maximum power operations in the current plane. The operation points are marked by 'O'. From zero to 2400rpm, the points represent the maximum torque locus. From 2400 to 3600rpm, the points representing the maximum power follow the current limit circle. Above 3600rpm, the maximum power points are found at the points where the voltage limit and torque lines are met tangentially. Similar plots appeared in the previous works [8].

4. LMC Based Controller and Experimental Setup

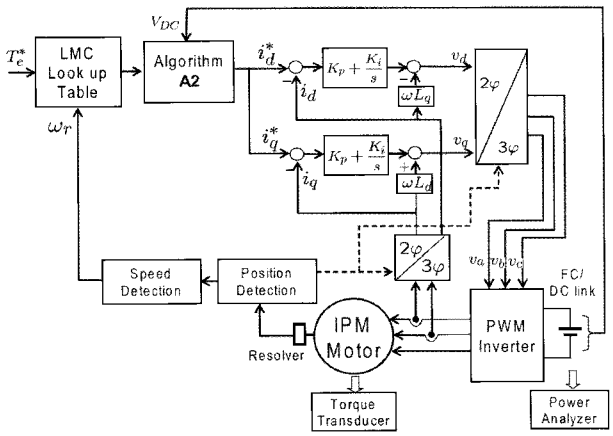

Fig. 4. The LMC structure for the FCEV PMSM

Fig. 4 shows a PMSM controller for a FCEV which includes the LMC table. The LMC table requires torque and speed as the input variables, and provides the optimal current commands. The LMC table is made for the largest possible DC link voltage in operation. However, the table output values are checked to find whether or not they are feasible under a given DC link voltage. If it is not feasible, then the output values are adjusted according to algorithm (A2). Next, the table output values are used for the current commands which minimize the motor loss for a given speed, torque, and DC link voltage. Conventional PI controllers can be used for d and q-axis current control along with decoupling and back-emf compensation.

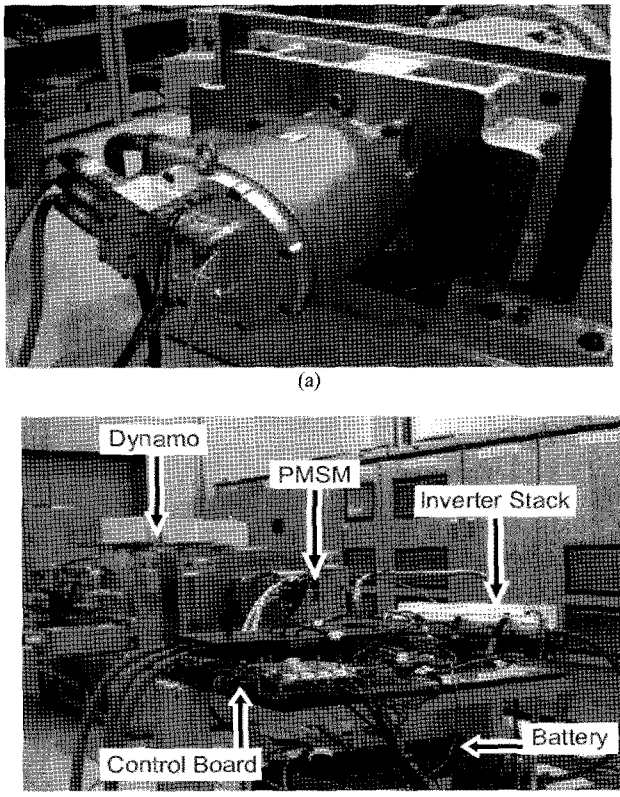

(a)

(b)

Fig. 5. Photos of (a) the FCEV PMSM and (b) experimental setup

The experimental environment is shown in Fig. 5. The proposed LMC were implemented utilizing a floating-point DSP (MPC5554). The PWM switching frequency was selected to be 8 kHz and the dead time 2μs. Current control routine was carried out every 125 μs, and torque command was refreshed at every 1.25ms. The PMSM was controlled in the torque mode by the inverter, and the dynamo motor (induction motor) was controlled in a speed control mode. A power analyzer was installed at the DC link side to monitor the input power $(V_{DC} \cdot I_{DC})$. A torque transducer installed between the two motors was used to measure the shaft torque. Through multiplying the measured torque by motor speed, shaft power $(T_e \cdot \omega_r)$ is obtained. Since the power analyzer reads the DC link power, the inverter loss has to be taken out to obtain the motor loss, i.e., the motor loss is measured according to

$$P_t^{meas} = V_{DC} I_{DC} - T_e \omega_r - P_{inv}$$

where P_{inv} is the inverter loss. P_{inv} is estimated by considering the IGBT on-drop and switching loss: The conduction loss is given by $P_{cond} = 6 \times \frac{2}{\pi} V_{ce}^{on} I_{phase}$, where V_{ce}^{on} is the IGBT on-drop voltage and I_{phase} is the peak value of the phase current. On the other hand, the switching loss P_{sw} is calculated according to $P_{sw} = E_{ts} f_{sw}$, where E_{ts} is the sum of IGBT turn on and off losses per a single PWM pulse, and f_{sw} is the PWM switching frequency.

5. Experimental Results

The parameters of the PMSM used in the experiment are summarized in Table 1. Loss coefficients, C_{fe} and C_{str} shown in Table 2 were tuned from those in [5] based on experimental results.

Table 2. Parameters of a PMSM for FCEV

Iron loss coefficient (c_{fe})	2.1×10^{-2}
Stray loss coefficient (C_{str})	3.0×10^{-8}

Instead of utilizing algorithms (A1) and (A2), the loss minimizing current sets can be found by an experimental method which scans the motor loss at each mesh point in the current plane. Similar experimental search method was utilized in finding MTPA solutions. [12].

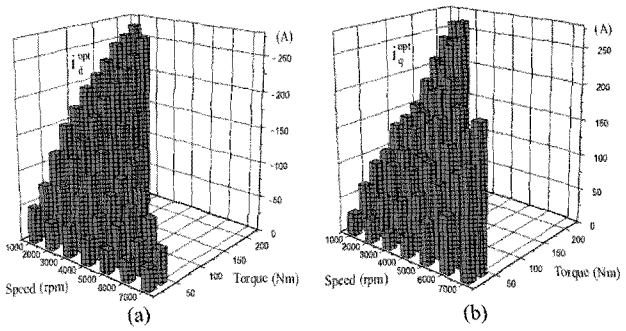

(a) (b)

Fig. 6. Photos of (a) the FCEV PMSM and (b) experimental setup

Fig. 6 shows the loss minimizing currents (i_d, i_q) for different speed and torque conditions found by the experimental scanning method. Fig. 7 shows motor loss P_t under constant torque conditions (a), (b), and (c), and under constant q-axis current conditions (d), (e), and (f). It is noted that the simulation results (dashed line) match well with the experimental results (symbols). Under constant torque condition, the loss decreases as $-i_d$ increases, and then it increases after passing an optimal i_d value. With fixed i_q conditions, the loss increases steadily as $-i_d$ increases.

Fig. 8 shows the loss minimizing (i_d, i_q) under fixed speeds 1000 ~ 6000rpm, while the torque is increasing. It compares the loss minimizing data obtained from the experimental scanning method with those from algorithms (A1) and (A2) (symbols: experimental results, dashed line: computed results). This shows that the two methods yield the same results. Fig. 8 also shows the contour of MTPA. Note again that MTPA is independent of the speed, and thus it cannot reflect the iron loss or the stray loss which are dependent upon the speed. The LMC results at 1000rpm are similar to those of MTPA.

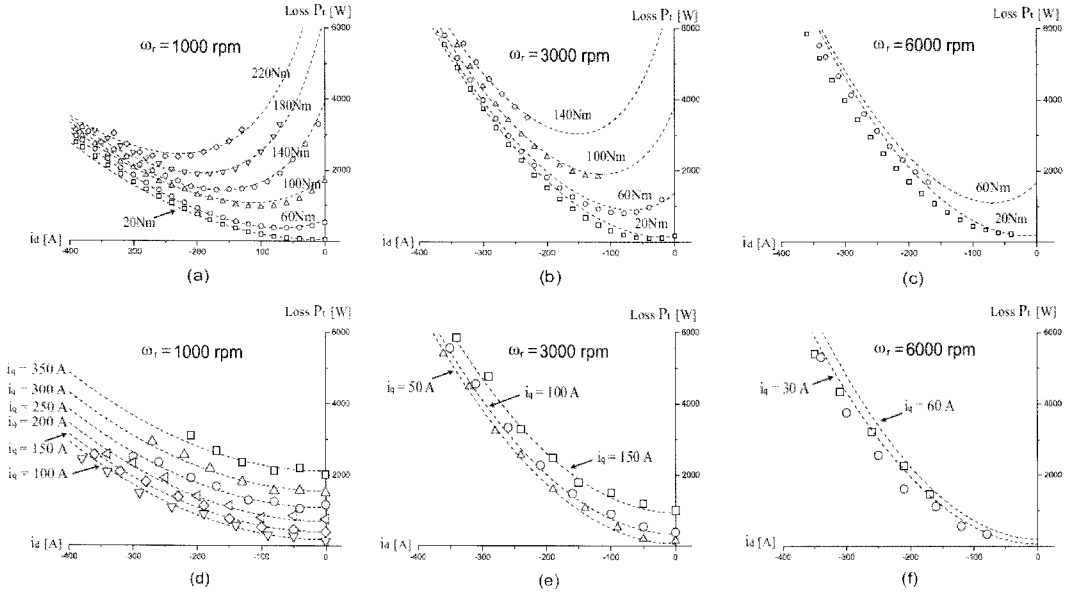

Fig. 7. The (total) motor loss under constant torque conditions (a),(b) and (c), and under constant q-axis current condition (d),(e) and (f). Symbols: experimental results, dashed line: computed result.

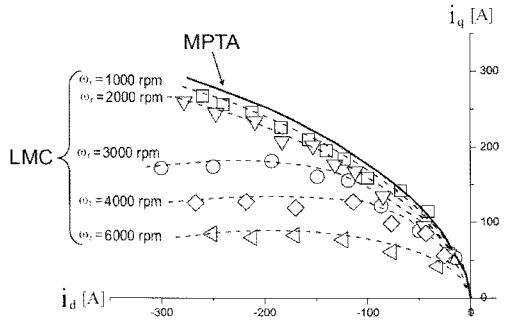

Fig. 8. Loss minimizing (i_d, i_q) under fixed speeds 1000, 3000 and 6000rpm, while the torque is increasing. Symbols: experimental results, dashed line: computed result.

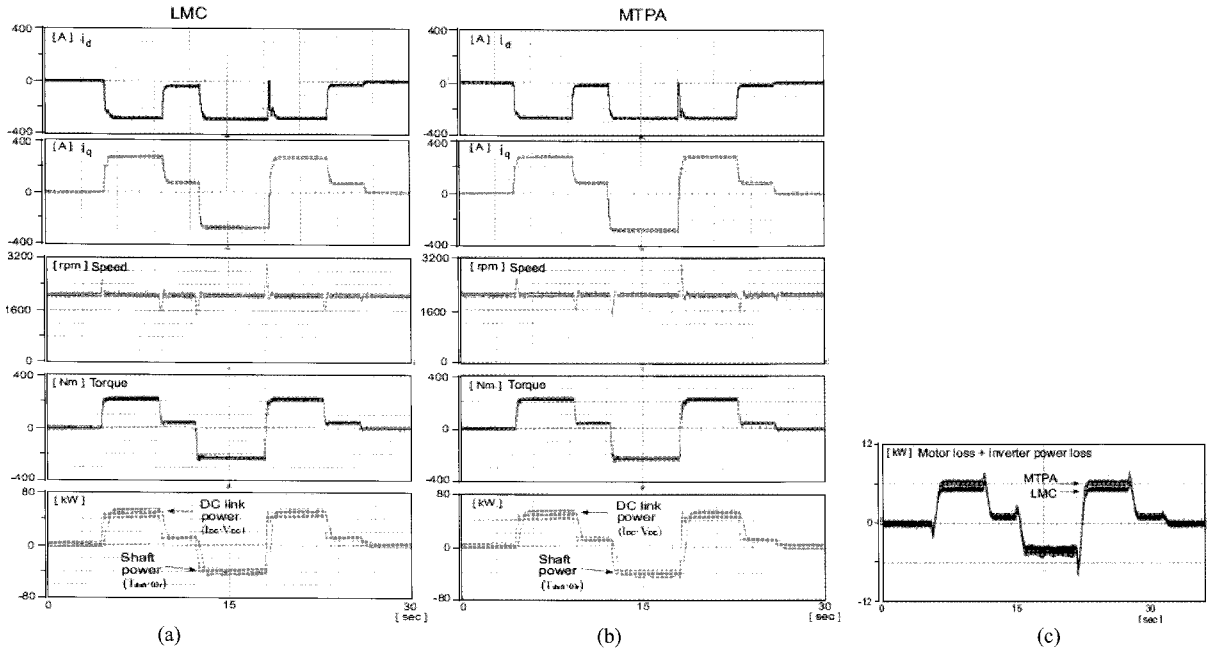

Fig. 9. Current response when torque changes at 2000rpm: (a) LMC, (b) MTPA and (c) the loss comparison.

Fig. 9 shows the plots of responses to a varying torque at constant speed (2000rpm). Note that both i_d and i_q change when torque varies. It displays the plots of measured shaft power and DC link power. The LMC results were compared to those of MTPA. Note from Fig. 9 (c) that LMC yielded lower loss than MTPA.

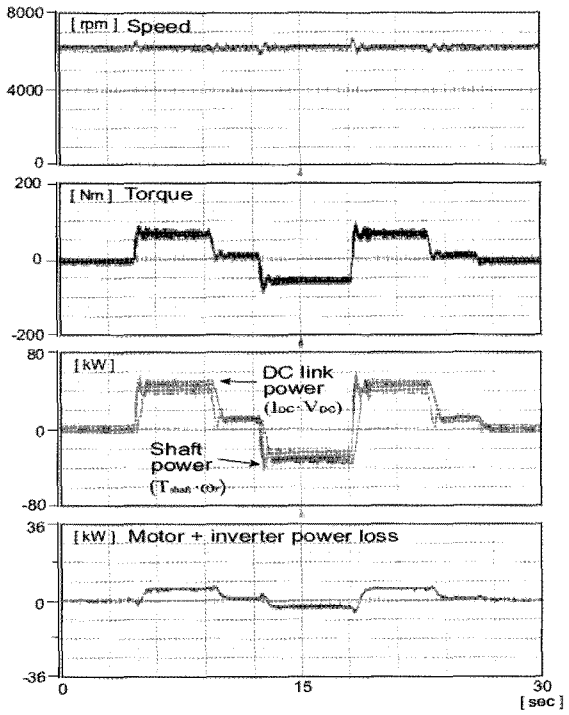

Fig. 10. The responses to torque variation at 6000rpm

Fig. 10 shows the same plots obtained by the LMC, but at 6000rpm. No MTPA solution is obtained at this torque and speed.

Fig. 11 shows the responses when the operating points move along the maximum torque and maximum power contours with the LMC. Fig. 11 (b) shows the current contour in the d, q current plane which corresponds to speed, torque, power, and loss plots shown in Fig. 11 (a). During the period from the origin (start) to the point O, torque was increased rapidly to the maximum (400A). Then to meet the power rating of the inverter, the current magnitude was decreased to 300A (Point P). Then, the points followed the current limit line with the increase in speed (Point Q). Fig. 11 (c) shows the computed result of the current trajectory.

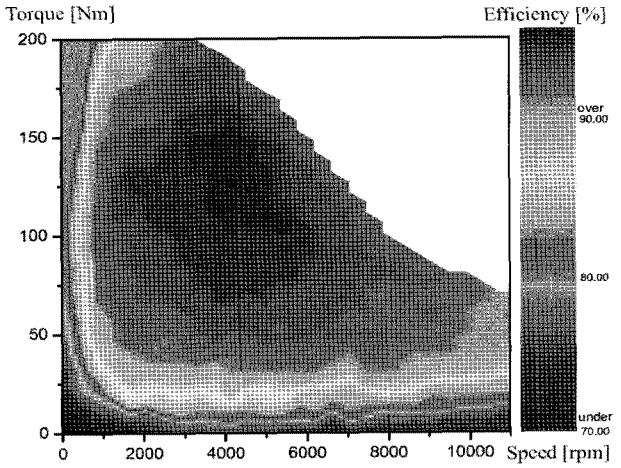

Fig. 12. Efficiency map for the PMSM for FCEV.

Finally, Fig. 12 shows the colored efficiency map of the motor. Efficiency ranges above 90% in most torque-speed region, but it is low in the low speed/low torque region

6. Concluding Remarks

A loss minimization control strategy was proposed for PMSMs. The motor loss function was set up, and the coefficients were found based on experimental data. The validated loss model was used for deriving a necessary condition for optimality. The optimal condition ended up with a

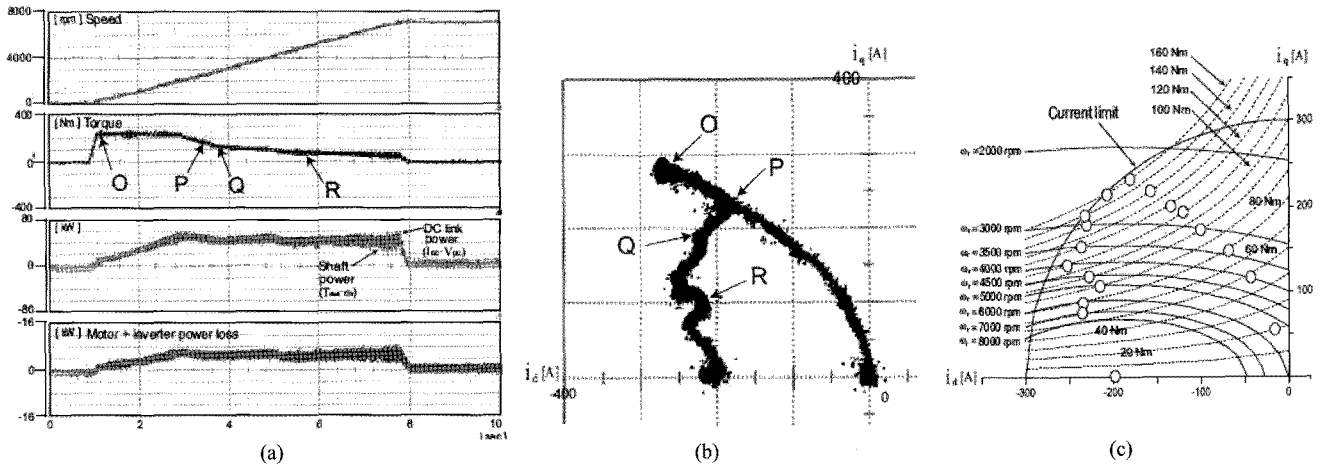

Fig. 11. Excursion along maximum torque and maximum power contour with LMC control: (a) Speed, torque, power and loss plots, (b) Current contour in d,q current plane, (c) Computed current trajectory.

fourth order polynomial in i_d. A zero crossing point of the polynomial was shown to be the loss minimizing point. The calculated minimizing solutions were compared with the values obtained from an experimental scanning method. The two results agreed in most torque-speed range. In addition, the loss minimizing data were made into a look-up table, and used for constructing an LMC. The proposed LMC provides the loss minimizing current commands in all operating range, and has an ability of adjusting to the varying DC-link voltage.

References

[1] C. C. Mi, G. R. Slemon, and R. Bonert, "Minimization of iron losses of permanent magnet synchronous machines," *IEEE Trans. on Energy Convers.*, vol. 20, no. 1, pp.121-127, Mar. 2005.

[2] Y. Nakamura, F. Ishibashi, and S. Hibino, "High-efficiency drive due to power factor control of a permanent magnet synchronous motor" *IEEE Trans. Power Electron.*, vol 10, Issue 2, pp.247-253, Mar. 1995.

[3] S. Morimoto, Y. Tong, Y. Takeda, and T. Hirasa, "Loss minimization control of permanent magnet synchronous motor drives," *IEEE Trans. Ind. Electron.*, vol. 41, Issue 5, pp.511-517, Oct. 1994.

[4] C. Mademlis, and N. Margaris, "Loss minimization in vector-controlled interior permanent-magnet synchronous motor drives," *IEEE Trans. Ind. Electron.*, vol. 49, Issue 6, pp.1344-1347, Dec. 2002.

[5] C. Mademlis, I. Kioskeridis, and N. Margaris, "Optimal efficiency control strategy for interior permanent-magnet synchronous motor drives," *IEEE Trans. Energy Convers.*, vol. 19, no. 4, pp.715-722, Dec. 2004

[6] F. Fernandez-Bernal, A. Garcia-Cerrada, and R. Faure, "Determination of parameters in interior permanent-magnet synchronous motors with iron losses without torque measurement," *IEEE Trans. Ind. Appl.*, vol. 36, Issue 3, pp.755-763 May/June 2000.

[7] C. Cavallaro, A. O. D. Tommaso, R. Miceli, A. Raciti, G. R. Galluzzo, and M. Tranpanese, "Efficiency enhancement of permanent-magnet synchronous motor drives by online loss minimization approaches," *IEEE Trans. Ind. Electron.*, vol 52, Issue 4, pp.1153-1160, Aug. 2005.

[8] G. Gallegos-Lopez, F. S. Gunawan, and J. E. Walters, "Optimum torque control of permanent-magnet AC machines in the field-weakened region," *IEEE Trans. Ind. Appl.*, vol. 41, no. 4, pp.1020-1028, July/Aug. 2005.

[9] Y. Jeong, S. Sul, S. Hiti, and K. M. Rahman, "Online minimum-copperloss control of an interior permanent-magnet synchronous machine for automotive applications," *IEEE Trans. Ind. Appl.*, vol. 42, no. 5, pp.1222- 1229, Sept./Oct. 2006.

[10] J. F. Gieras and M. Wing, Permanent Magnet Motor Technonology, Design Applications, 2nd. Ed., Marcel, Dekker, Inc., New York, 2002.

[11] Ching-Tsai Pan and S. -M. Sue, "A linear maximum torque per ampere control for IPMSM drives over full-speed range," *IEEE Trans. Energy Convers.*, vol. 20, Issue 2, pp.359-366 June 2005.

[12] N. Bianchi, S. Bolognani, and M. Zigliotto, "High-performance PM synchronous motor drive for an electrical scooter," *IEEE Trans. Ind. Appl.*, vol. 19, Issue 4, pp.715-723, Dec. 2004.

[13] E. C. Lovelace, T. M. Jahns, and J. H. Lang, "Impact of saturation and inverter cost on interior PM synchronous machine drive optimization," *IEEE Trans. Ind. Appl.*, vol. 36, Issue 3, pp.723-729, May/June 2004.

[14] A. Haddoun, M. E. H. Benbouzid, D. Diallo, R. Abdessemed, J. Ghouili, and K. Srairi, "A loss-minimization DTC scheme for EV induction motors," *IEEE Trans. Vehicular Technology*, vol. 56, Issue 1, pp.81-88, Jan. 2007.

[15] S. Shinnaka, T. Sagawa, "New optimal current control methods for energy-efficient and wide speed-range operation of hybrid-field synchronous motor," *IEEE Trans. Ind. Electron.*, vol. 54, Issue 5, pp.2443-2450, Oct. 2007.

[16] J. Larminie and A. Dicks, Fuel Cell Systems Explained, 2nd. Ed. John Wiley & Sons, Inc., 2001.

[17] D.G. Luenberger, Linear and Nonlinaer Programming, Addison-Wesley Publishing Company, 1989.

Jung-Gi Lee

He was born in Jeonju, Korea in 1975 He received the B.S. degree in control and instrumentation engineering from Chonbuk national university, Jeonju, in 2002, and the M.S. and Ph.D degree in electrical engineering from POSTECH in 2004, 2009 respectively. He is currently working toward the Ph.D. degree in electrical engineering.

His current research interests include design, analysis and control of power electronic systems, ac motor drives, electric vehicles, and fuel cell systems.

Kwang-Hee Nam

He was born in Seoul, Korea in 1956. He recieved the B.S. degree in chemical technology and M.S. degree in control and instrumentation engineering from Seoul national university, Seoul, in 1980 and 1982, respectively. and M.S. degree in mathematics and Ph. D degree in electrical engineering from the University of Texas at Austin, in 1986.

From 1998 to 2000, He was the Director of the Information Research Laboratories and the Dean of the Graduate school of Information Technology, Pohang University of Science and technology (POSTECH), Pohang, Korea, where he is currently a Professor in the Department of Electrical Engineering. His current research interests include ac motor control, power converters, electric vehicles, computer networks, fuel cell systems, and nonlinear system analysis.
Prof. Nam received the IEEE Transactions on Industrial Electronics Best Paper Award in 2000.

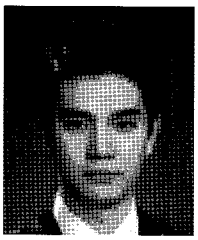

Sun-Ho Lee
He was born in Seoul, Korea in 1981. He recieved the B.S. degree in mechanical engineering from Hongik university, Seoul in 2008 He is currently working toward the M.S. degree in electrical engineering at POSTECH, Pohang, Korea.
His current research interests include design, analysis and control of power electronic systems, ac motor drives.

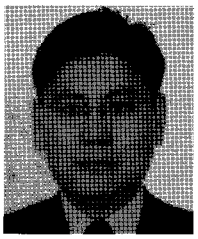

Soe-Ho Choi
He was born in Seoul, Korea in 1970. He recieved the B.S. degree in mechanical engineering from Korea university, Inchoen in 1992 and M.S. and Ph.d. degree in mechanical engineering from KAIST in 1995, 2000 respectively. He is currently a working group leader in performance development and control of fuel cell vehicle group in Hyundai motor company.
His main research interests are power distribution control of fuel cell and battery/super-cap hybrid vehicle, fuel cell system control, traction motor control of IPM and induction motor.

Soon-Woo Kwon
He was born in Seoul, Korea in 1973. He recieved the B.S. degree in mechanical engineering from Inha university, Inchoen in 1996 and M.S. degree in applied control from KAIST. He is currently a senior research engineer in Hyundai motor company.
His main research interests are power distribution control of fuel cell and battery hybrid vehicle, theory of optimal and robust control, traction motor control of IPM and induction motor.